frontiers | Frontiers in Physics

TYPE Brief Research Report
PUBLISHED 10 February 2023
DOI 10.3389/fphy.2023.1129933

Check for updates

OPEN ACCESS

EDITED BY
Xiaoming Zhang,
Hebei University of Technology, China

REVIEWED BY
Jiangchao Han,
Beihang University, China
Mingmin Zhong,
Southwest University, China

*CORRESPONDENCE
Yang Li,
liyang_physics@126.com

SPECIALTY SECTION
This article was submitted to Condensed Matter Physics,
a section of the journal
Frontiers in Physics

RECEIVED 22 December 2022
ACCEPTED 23 January 2023
PUBLISHED 10 February 2023

CITATION
Li Y (2023), Multiple Weyl and double-Weyl points in the phonon dispersion of $P4_332$ $BaSi_2$.
*Front. Phys.* 11:1129933.
doi: 10.3389/fphy.2023.1129933

COPYRIGHT
© 2023 Li. This is an open-access article distributed under the terms of the Creative Commons Attribution License (CC BY). The use, distribution or reproduction in other forums is permitted, provided the original author(s) and the copyright owner(s) are credited and that the original publication in this journal is cited, in accordance with accepted academic practice. No use, distribution or reproduction is permitted which does not comply with these terms.

# Multiple Weyl and double-Weyl points in the phonon dispersion of $P4_332$ $BaSi_2$

Yang Li[1,2]*

[1]Aviation and Automobile School, Chongqing Youth Vocational and Technical College, Chongqing, China, [2]College of Physics, Chongqing University, Chongqing, China

Weyl semimetals, classified as solid-state crystals and whose Fermi energy is accurately situated at Weyl points (WPs), have received much attention in condensed matter physics over the past 10 years. Weyl quasiparticles have been observed in the electronic and bosonic regimes, in addition to the extensive amount of theoretical and numerical predictions for the Weyl semimetals. This study demonstrates that 12 single Weyl phonons with linear dispersion and six double Weyl phonons with quadratic dispersion coexist between two specific phonon branches in real material $P4_332$ $BaSi_2$. The 12 single Weyl phonons and the six double Weyl phonons can form a Weyl complex phonon, which hosts a zero net chirality.

KEYWORDS

**DFPT calculation, phonon, Weyl point, DFT, topological feature**

## Introduction

Condensed-matter systems with inherent topological orders have received a great deal of attention lately. On the one hand, since quasiparticle excitations in realistic materials provide analogs of relativistic fermions or bosons in quantum field theory, these topological systems offer exotic platforms to study elementary particles and their related phenomena in high-energy physics. However, non-trivial topology, which is characterized by topological invariants, gives rise to topological quasiparticles in crystalline solids [1], providing an intriguing way to study symmetry-protected topological orders. Additionally, the crystal symmetry rather than the Poincare symmetry constraints quasiparticles in crystalline solids. There is therefore a possibility of discovering unusual topological quasiparticles [2–10] without high-energy physics counterparts in condensed-matter physics in addition to the traditional Dirac, Weyl, and Majorana particles in the standard model.

Numerous conventional and non-conventional topological quasiparticles have been proposed up to this point. For instance, intense research focuses on topological bosons in crystalline solids and various non-trivial fermions in topological semimetals [11–29]. Weyl-type excitations stand out among these non-trivial quasiparticles as being particularly significant. A quantized chiral charge, also known as the Chern number *C*, is what defines the topology of a Weyl point (WP). WPs are present in a system by shattering either the time-reversal or inversion symmetry because of the twofold-degenerate feature.

However, the crystal symmetries of crystalline solids are more intricate and may contain unusual Weyl-type quasiparticles. For example, the screw rotational symmetry can protect double WPs or WPs with the higher Chern number *C*. The 4-fold or 6-fold rotational symmetry can protect quadratic-double or cubic-triple WPs [28, 30–39].

This work identifies a Weyl complex composed of 12 C-1 WPs and 6 C-2 WPs in the phonon dispersion for $P4_332$ $BaSi_2$. Note that $P4_332$ $BaSi_2$ is a prepared experiential material [40]. $BaSi_2$ crystallizes in the cubic $P4_3232$ space group. $Ba^{2+}$ is bonded in an 8-coordinate

geometry to eight equivalent $Si^{1-}$ atoms. $Si^{1-}$ is bonded in a 7-coordinate geometry to four equivalent $Ba^{2+}$ and three equivalent $Si^{1-}$ atoms. The optimized lattice constants for $P4_332$ $BaSi_2$ are a = b = c = 6.771 Å, which are in good agreement with the experimental data, i.e., a = b = c = 6.715 Å [40]. The crystal structure of the relaxed $BaSi_2$ is shown in Figure 1A.

## Methods

Using the Vienna *ab initio* Simulation Package [41] and the DFT framework, computations for the realistic material $BaSi_2$ were carried out. The calculation's energy and force convergence conditions were set to $10^{-6}$ eV and −0.01 eV/Å, respectively. A 5 × 5 × 5 Monkhorst-Pack grid was used to sample the whole BZ after the plane-wave expansion was truncated at 500 eV. We used the density functional perturbation theory to obtain the force constants for phonon spectrum calculations, and then we used the PHONOPY package [42] to calculate the phonon dispersion spectrum. We obtained the phonon Hamiltonian of the tight-binding model and the surface local DOSs with the open-source software WANNIER TOOLS [50] and surface Green's functions.

## Results and discussion

We determine the phonon spectra using first-principles calculations and verify that the two obvious phonon crossing points are present in the optical phonon branches of $P4_332$ $BaSi_2$. The absence of an imaginary frequency in the phonon spectrum, as seen in Figure 1C, demonstrates the $P4_332$ $BaSi_2$'s dynamical stability. We mainly focus on the frequencies around 8 THz and find two obvious phonon crossing points, P1 and P2, on Γ-X and Γ-M, respectively (see Figure 1B).

Figures 2A, B display the three-dimensional plot of the twofold degenerate phonon bands around the P1 and P2 points, respectively. From Figure 2A, one finds that the WP at P1 is a Charge-two WP. The charge-2 Weyl point (C-2 WP) is a topologically charged 0D two-fold band degeneracy with a charge of 2. It has a quadratic energy splitting in the plane perpendicular to the Γ-X direction and a linear dispersion in one direction (Γ-X). On a high-symmetry line or at a high-symmetry point in the BZ, the C-2 WP can happen. Figure 2B shows that the WP at P2 is a Charge-one WP. The charge-1 Weyl point (C-1 WP) is a degeneracy of the 0D two-fold band. It can occur at a generic *k* point in BZ and features a linear energy splitting in any direction in momentum space.

Note that C-2 WP and C-1 WP are also named as double WP and single WP, respectively. In the scientific literature, double-Weyl points with greater topological ordering and emerging in particular crystals with particular symmetries have been discovered. Because double-Weyl points result from the coalescence of two single-Weyl points, their topological charge values are equal to 2 and −2.

In order to determine the chirality of Weyl phonons, we employ the Wilson-loop method within the evolution of the average position of Wannier centers. Figures 2C, D show the evolution of the average position of the Wannier centers for the P1 WP with positive chirality

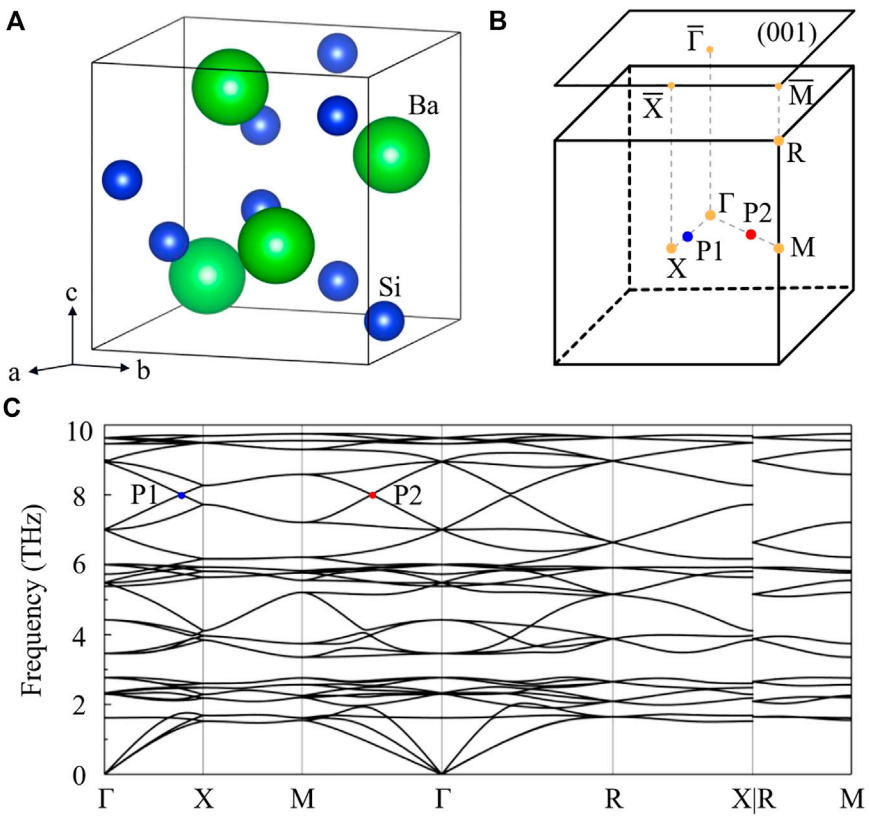


FIGURE 1
**(A)** The crystal structure for $BaSi_2$. **(B)** 3D bulk and 2D surface BZs. **(C)** Phonon dispersion for $BaSi_2$. P1 and P2 are two obvious crossing points.

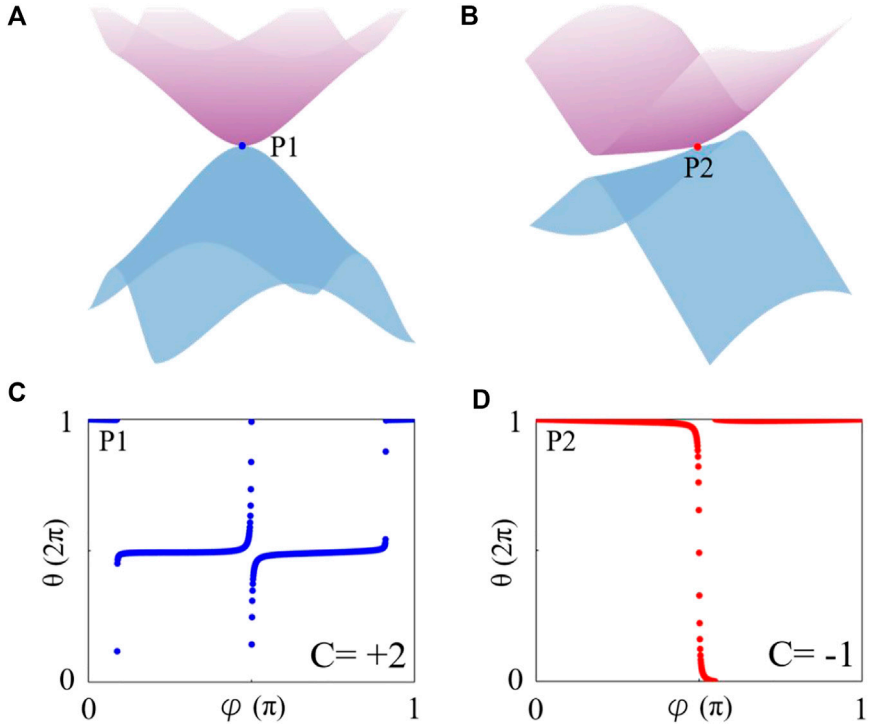


FIGURE 2
**(A)** and **(B)** 3D plots of the phonon bands around P1 and P2 points. **(C)** and **(D)** Evolutions of the average position of the Wannier center for the WP with C = +2 at P1 and the WP with C = −1 at P2.

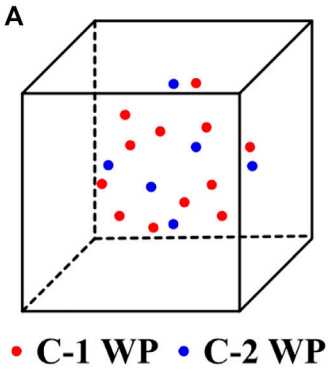


B

| No. | Momentum position | Chern number | No. | Momentum position | Chern number |
|---|---|---|---|---|---|
| 1 | (0.3861, 0, 0) | +2 | 4 | (-0.2503, -0.2503, 0) | -1 |
| 2 | (-0.3861, 0, 0) | +2 | 5 | (0.2503,0, 0.2503) | -1 |
| 3 | (0, 0.3861, 0) | +2 | 6 | (-0.2503,0, -0.2503) | -1 |
| 4 | (0, -0.3861, 0) | +2 | 7 | (-0.2503,0, 0.2503) | -1 |
| 5 | (0, 0, 0.3861) | +2 | 8 | (0.2503,0, -0.2503) | -1 |
| 6 | (0, 0, -0.3861) | +2 | 9 | (0, 0.2503, 0.2503) | -1 |
| 1 | (0.2503, 0.2503, 0) | -1 | 10 | (0, -0.2503, 0.2503) | -1 |
| 2 | (-0.2503, 0.2503, 0) | -1 | 11 | (0, 0.2503, -0.2503) | -1 |
| 3 | (0.2503, -0.2503, 0) | -1 | 12 | (0, -0.2503, -0.2503) | -1 |

FIGURE 3
**(A)** and **(B)** positions for the 12 C-1 WPs and 6 C-2 WPs in the 3D BZ.

and the evolution of the average position of the Wannier centers for the P2 WP with negative chirality, respectively. These findings suggest that the WP at P1 (or P2) forms a double phonon WP with chiral charge 2 (or a single WP with chiral charge −1).

As shown in Figure 3A, one finds a total of 12 single WPs with C = −1 and 6 double WPs with C = +2 in the 3D BZ. The positions for all these multiple C-1 and C-2 WPs are shown in Figure 3B. These 12 C-1 WPs and 6 C-2 WPs will form a Weyl complex, which has a zero net chiral charge and obeys the Nielsen-Ninomiya no-go theorem [51, 52]. Note that the Weyl compelx has also be predicted by series research groups [53–56].

Therefore, our findings present ideal candidates for C-1 and C-2 WP phonons to form phononic Weyl complexes. Moreover, our findings are applicable to fermionic systems.

Unique non-trivial surface states are associated with the exotic C-2 and C-1 WP phonons. We build a phonon tight-binding Hamiltonian in the Wannier representation using second-order interatomic force constants to demonstrate this. The iterative Green's function method is used to calculate phonon surface states in this model. Figure 4 depicts the local phonon density of states (LDOS) projected on a semi-infinite (001) surface of $P4_332$ $BaSi_2$. As anticipated, there are two visible phonon surface states, each of which begins at the projection of the double WP and

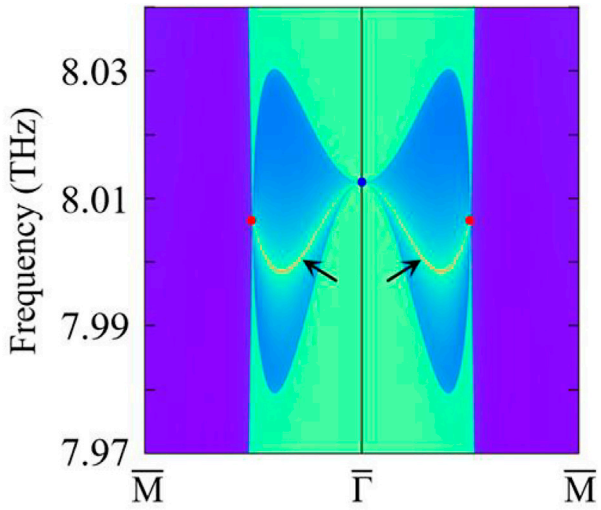


FIGURE 4
The phonon LDOS projected on the (001) surface. The phonon surface states are marked by black arrows.

ends at the projections of two single WPs. The lack of trivial bulk states on the (001) surface of $P4_332$ $BaSi_2$ substantially simplifies experimental detection and subsequent applications [43–49].

## Summary

We demonstrated that in real material $P4_332$ $BaSi_2$, there are 12 single WPs with C = −1 and 6 double WPs with C = +2 in the 3D BZ. These Weyl phonons create a Weyl complex with zero net charge number, and their non-trivial surface states connect the projections of phonon WPs are visible.

## Data availability statement

The raw data supporting the conclusion of this article will be made available by the authors, without undue reservation.

## Author contributions

Investigations and writing: YL.

## Funding

This work is supported by the Science and Technology Research Program of Chongqing Municipal Education Commission (Grant Nos. KJZD-K202104101 and KJQN202204104) and the school-level Scientific Research Project of Chongqing Youth Vocational and Technical College (Grant No. CQY2021KYZ03).

## Conflict of interest

The author declares that the research was conducted in the absence of any commercial or financial relationships that could be construed as a potential conflict of interest.

## Publisher's note

All claims expressed in this article are solely those of the authors and do not necessarily represent those of their affiliated organizations, or those of the publisher, the editors and the reviewers. Any product that may be evaluated in this article, or claim that may be made by its manufacturer, is not guaranteed or endorsed by the publisher.

## References

1. Yu ZM, Zhang Z, Liu GB, Wu W, Li XP, Zhang RW, et al. Encyclopedia of emergent particles in three-dimensional crystals. *Sci Bull* (2022) 67(4):375–80. doi:10.1016/j.scib.2021.10.023

2. Yan B, Felser C. Topological materials: Weyl semimetals. *Annu Rev Condensed Matter Phys* (2017) 8:337–54. doi:10.1146/annurev-conmatphys-031016-025458

3. Lv BQ, Weng HM, Fu BB, Wang XP, Miao H, Ma J, et al. Experimental discovery of weyl semimetal TaAs. *Phys Rev X* (2015) 5(3):031013. doi:10.1103/physrevx.5.031013

4. Soluyanov AA, Gresch D, Wang Z, Wu Q, Troyer M, Dai X, et al. Type-ii weyl semimetals. *Nature* (2015) 527(7579):495–8. doi:10.1038/nature15768

5. Hosur P, Qi X. Recent developments in transport phenomena in Weyl semimetals. *Comptes Rendus Physique* (2013) 14(9-10):857–70. doi:10.1016/j.crhy.2013.10.010

6. Chan CK, Lindner NH, Refael G, Lee PA. Photocurrents in weyl semimetals. *Phys Rev B* (2017) 95(4):041104. doi:10.1103/physrevb.95.041104

7. Wang HX, Lin ZK, Jiang B, Guo GY, Jiang JH. Higher-order weyl semimetals. *Phys Rev Lett* (2020) 125(14):146401. doi:10.1103/physrevlett.125.146401

8. Ruan J, Jian SK, Zhang D, Yao H, Zhang H, Zhang SC, et al. Ideal weyl semimetals in the ChalcopyritesCuTlSe2,AgTlTe2,AuTlTe2, andZnPbAs2. *Phys Rev Lett* (2016) 116(22):226801. doi:10.1103/physrevlett.116.226801

9. Armitage NP, Mele EJ, Vishwanath A. Weyl and Dirac semimetals in three-dimensional solids. *Rev Mod Phys* (2018) 90(1):015001. doi:10.1103/revmodphys.90.015001

10. Young SM, Kane CL. Dirac semimetals in two dimensions. *Phys Rev Lett* (2015) 115(12):126803. doi:10.1103/physrevlett.115.126803

11. Zhang X, Jin L, Dai X, Liu G. Topological type-II nodal line semimetal and Dirac semimetal state in stable kagome compound $Mg_3Bi_2$. *J Phys Chem Lett* (2017) 8(19):4814–9. doi:10.1021/acs.jpclett.7b02129

12. Wang L, Yang Y, Wang J, Liu W, Liu Y, Gong J, et al. Excellent catalytic performance toward the hydrogen evolution reaction in topological semimetals. *EcoMat* (2022) 2022:e12316. doi:10.1002/eom2.12316

13. Tian L, Liu Y, Meng W, Zhang X, Dai X, Liu G. Spin–orbit coupling-determined topological phase: Topological insulator and quadratic Dirac semimetals. *J Phys Chem Lett* (2020) 11(24):10340–7. doi:10.1021/acs.jpclett.0c03103

14. Meng W, Zhang X, He T, Jin L, Dai X, Liu Y, et al. Ternary compound HfCuP: An excellent Weyl semimetal with the coexistence of type-I and type-II Weyl nodes. *J Adv Res* (2020) 24:523–8. doi:10.1016/j.jare.2020.05.026

15. Chen DY, Wu Y, Jin L, Li Y, Wang X, Duan J, et al. Superconducting properties in a candidate topological nodal line semimetal SnTaS2 with a centrosymmetric crystal structure. *Phys Rev B* (2019) 100(6):064516. doi:10.1103/physrevb.100.064516

16. Liu G, Jin L, Dai X, Chen G, Zhang X. Topological phase with a critical-type nodal line state in intermetallic CaPd. *Phys Rev B* (2018) 98(7):075157. doi:10.1103/physrevb.98.075157

17. Wang X, Ding G, Cheng Z, Surucu G, Wang XL, Yang T. Rich topological nodal line bulk states together with drum-head-like surface states in NaAlGe with anti-PbFCl type structure. *J Adv Res* (2020) 23:95–100. doi:10.1016/j.jare.2020.01.017

18. Wang X, Ding G, Cheng Z, Surucu G, Wang XL, Yang T. Novel topological nodal lines and exotic drum-head-like surface states in synthesized CsCl-type binary alloy TiOs. *J Adv Res* (2020) 22:137–44. doi:10.1016/j.jare.2019.12.001

19. Wang X, Cheng Z, Zhang G, Kuang M, Wang XL, Chen H. Strain tuning of closed topological nodal lines and opposite pockets in quasi-two-dimensional α-phase FeSi2. *Phys Chem Chem Phys* (2020) 22(24):13650–8. doi:10.1039/d0cp02334e

20. Yang T, Jin L, Liu Y, Zhang X, Wang X. Spin-polarized type-II nodal loop and nodal surface states in hexagonal compounds $XTiO_2$ (X= Li, Na, K, Rb). *Phys Rev B* (2021) 103(23):235140. doi:10.1103/physrevb.103.235140

21. Zhou F, Liu Y, Kuang M, Wang P, Wang J, Yang T, et al. Time-reversal-breaking Weyl nodal lines in two-dimensional $A_3C_2$ (A= Ti, Zr, and Hf) intrinsically ferromagnetic materials with high Curie temperature. *Nanoscale* (2021) 13(17):8235–41. doi:10.1039/d1nr00139f

22. Wang X, Cheng Z, Zhang G, Yuan H, Chen H, Wang XL. Spin-gapless semiconductors for future spintronics and electronics. *Phys Rep* (2020) 888:1–57. doi:10.1016/j.physrep.2020.08.004

23. Zhou F, Liu Y, Wang J, Kuang M, Yang T, Chen H, et al. Intersecting topological nodal ring and nodal wall states in superhard superconductor $FeB_4$. *Phys Rev Mater* (2021) 5(7):074201. doi:10.1103/physrevmaterials.5.074201

24. Xie C, Yuan H, Zhang Z, Wang X. Magnetic Weyl and quadratic nodal lines in inverse-Heusler-based fully compensated ferrimagnetic half-metals. *Phys Rev Mater* (2022) 6(9):094406. doi:10.1103/physrevmaterials.6.094406

25. Gao H, Venderbos JW, Kim Y, Rappe AM. Topological semimetals from first principles. *Annu Rev Mater Res* (2019) 49:153–83. doi:10.1146/annurev-matsci-070218-010049

26. Bernevig A, Weng H, Fang Z, Dai X. Recent progress in the study of topological semimetals. *J Phys Soc Jpn* (2018) 87(4):041001. doi:10.7566/jpsj.87.041001

27. Fang C, Lu L, Liu J, Fu L. Topological semimetals with helicoid surface states. *Nat Phys* (2016) 12(10):936–41. doi:10.1038/nphys3782

28. Fang C, Gilbert MJ, Dai X, Bernevig BA. Multi-Weyl topological semimetals stabilized by point group symmetry. *Phys Rev Lett* (2012) 108(26):266802. doi:10.1103/physrevlett.108.266802

29. Ding G, Wang J, Yu ZM, Zhang Z, Wang W, Wang X. Single pair of type-III weyl points half-metals: BaNiIO6 as an example. *Phys Rev Mater* (2023) 7(1):014202. doi:10.1103/physrevmaterials.7.014202

30. Zhang T, Song Z, Alexandradinata A, Weng H, Fang C, Lu L, et al. Double-Weyl phonons in transition-metal monosilicides. *Phys Rev Lett* (2018) 120(1):016401. doi:10.1103/physrevlett.120.016401

31. Miao H, Zhang TT, Wang L, Meyers D, Said AH, Wang YL, et al. Observation of double Weyl phonons in parity-breaking FeSi. *Phys Rev Lett* (2018) 121(3):035302. doi:10.1103/physrevlett.121.035302

32. Lai HH. Correlation effects in double-Weyl semimetals. *Phys Rev B* (2015) 91(23):235131. doi:10.1103/physrevb.91.235131

33. Jian SK, Yao H. Correlated double-Weyl semimetals with Coulomb interactions: Possible applications to $HgCr_2Se$ 4 and $SrSi_2$. *Phys Rev B* (2015) 92(4):045121. doi:10.1103/physrevb.92.045121

34. Chen Q, Fiete GA. Thermoelectric transport in double-Weyl semimetals. *Phys Rev B* (2016) 93(15):155125. doi:10.1103/physrevb.93.155125

35. Wang YT, Tsai YW. Multiple Weyl and double-Weyl points in an elastic chiral lattice. *New J Phys* (2018) 20(8):083031. doi:10.1088/1367-2630/aada55

36. Zhong M, Han Y, Wang J, Liu Y, Wang X, Zhang G. Material realization of double-Weyl phonons and phononic double-helicoid surface arcs with P213 space group. *Phys Rev Mater* (2022) 6(8):084201. doi:10.1103/physrevmaterials.6.084201

37. Ding G, Zhou F, Zhang Z, Yu ZM, Wang X. Charge-two Weyl phonons with type-III dispersion. *Phys Rev B* (2022) 105(13):134303. doi:10.1103/physrevb.105.134303

38. Singh B, Chang G, Chang TR, Huang SM, Su C, Lin MC, et al. Tunable double-Weyl Fermion semimetal state in the $SrSi_2$ materials class. *Scientific Rep* (2018) 8(1):10540–9. doi:10.1038/s41598-018-28644-y

39. He H, Qiu C, Cai X, Xiao M, Ke M, Zhang F, et al. Observation of quadratic Weyl points and double-helicoid arcs. *Nat Commun* (2020) 11(1):1820–6. doi:10.1038/s41467-020-15825-5

40. Evers J, Oehlinger G, Weiss A. Eine neue hochdruckphase von Bariumdisilicid. *Angew Chem* (1978) 90(7):562–3. doi:10.1002/ange.19780900724

41. Hafner J. *Ab-initio* simulations of materials using VASP: Density-functional theory and beyond. *J Comput Chem* (2008) 29(13):2044–78. doi:10.1002/jcc.21057

42. Togo A, Tanaka I. First principles phonon calculations in materials science. *Scripta Materialia* (2015) 108:1–5. doi:10.1016/j.scriptamat.2015.07.021

43. Singh S, Wu Q, Yue C, Romero AH, Soluyanov AA. Topological phonons and thermoelectricity in triple-point metals. *Phys Rev Mater* (2018) 2(11):114204. doi:10.1103/physrevmaterials.2.114204

44. Liu Y, Chen X, Xu Y. Topological phononics: From fundamental models to real materials. *Adv Funct Mater* (2020) 30(8):1904784. doi:10.1002/adfm.201904784

45. Wang X, Zhou F, Yang T, Kuang M, Yu ZM, Zhang G. Symmetry-enforced ideal lanternlike phonons in the ternary nitride $Li_6WN_4$. *Phys Rev B* (2021) 104(4):L041104. doi:10.1103/physrevb.104.l041104

46. Xie C, Liu Y, Zhang Z, Zhou F, Yang T, Kuang M, et al. Sixfold degenerate nodal-point phonons: Symmetry analysis and materials realization. *Phys Rev B* (2021) 104(4):045148. doi:10.1103/physrevb.104.045148

47. Zhou F, Zhang Z, Chen H, Kuang M, Yang T, Wang X. Hybrid-type nodal ring phonons and coexistence of higher-order quadratic nodal line phonons in an AgZr alloy. *Phys Rev B* (2021) 104(17):174108. doi:10.1103/physrevb.104.174108

48. Xie C, Yuan H, Liu Y, Wang X, Zhang G. Three-nodal surface phonons in solid-state materials: Theory and material realization. *Phys Rev B* (2021) 104(13):134303. doi:10.1103/physrevb.104.134303

49. Feng Y, Xie C, Chen H, Liu Y, Wang X. Dirac point phonons at high-symmetry points: Towards materials realization. *Phys Rev B* (2022) 106(13):134307. doi:10.1103/physrevb.106.134307

50. Wu Q, Zhang S, Song HF, Troyer M, Soluyanov AA. WannierTools: An open-source software package for novel topological materials. *Comp Phys Commun* (2018) 224:405–16. doi:10.1016/j.cpc.2017.09.033

51. Nielsen HB, Ninomiya M. Absence of neutrinos on a lattice:(I). Proof by homotopy theory. *Nucl Phys B* (1981) 185(1):20–40. doi:10.1016/0550-3213(81)90361-8

52. Nielsen HB, Ninomiya M. Absence of neutrinos on a lattice:(II). Intuitive topological proof. *Nucl Phys B* (1981) 193(1):173–94. doi:10.1016/0550-3213(81)90524-1

53. Wang X, Zhou F, Zhang Z, Yu ZM, Yao Y. Hourglass charge-three Weyl phonons. *Phys Rev B* (2022) 106(21):214309. doi:10.1103/physrevb.106.214309

54. Liu QB, Wang Z, Fu HH. Charge-four weyl phonons. *Phys Rev B* (2021) 103(16):L161303. doi:10.1103/physrevb.103.l161303

55. Wang R, Xia BW, Chen ZJ, Zheng BB, Zhao YJ, Xu H. Symmetry-protected topological triangular Weyl complex. *Phys Rev Lett* (2020) 124(10):105303. doi:10.1103/physrevlett.124.105303

56. Huang Z, Chen Z, Zheng B, Xu H. Three-terminal Weyl complex with double surface arcs in a cubic lattice. *Npj Comput Mater* (2020) 6(1):87–7. doi:10.1038/s41524-020-00354-y